This is a repository copy of *A functional form for a representative individual arterial input function measured from a population using high temporal resolution DCE MRI*.

White Rose Research Online URL for this paper:
http://eprints.whiterose.ac.uk/136005/

Version: Accepted Version

Article:

Title:

A functional form for a representative individual arterial input function measured from a population using high temporal resolution dynamic contrast-enhanced MRI

Authors:

Dr Leonidas Georgiou, PhD, l.georgiou@leeds.ac.uk, Biomedical Imaging, University of Leeds, Leeds, UK and Department of Medical Physics, German Oncology Center, Limassol, Cyprus.

Dr Daniel J. Wilson, PhD, daniel.wilson8@nhs.net, Department of Medical Physics and Engineering, Leeds Teaching Hospital NHS Trust, Leeds, UK

Dr Nisha Sharma, MB, MRCP, FRCR, nisha.sharma2@nhs.net, Department of Radiology, Leeds Teaching Hospital NHS Trust, Leeds, UK

Prof. Timothy J. Perren, MD, FRCP, t.j.perren@leeds.ac.uk, Leeds Institute of Cancer and Pathology, St. James's University Hospital, Leeds, UK

Prof David L. Buckley, PhD, d.l.buckley@leeds.ac.uk, Biomedical Imaging, University of Leeds, Leeds, UK

Corresponding Author:

David L. Buckley, PhD

Biomedical Imaging, University of Leeds,

LIGHT Laboratories, Clarendon Way, Leeds, LS2 9JT, UK.

e-mail: d.l.buckley@leeds.ac.uk; tel. +44 113 343 2017

Running Title: A representative AIF for DCE-MRI studies

Word count: 3191

Abstract

Purpose: To measure the arterial input function (AIF), an essential component of tracer kinetic analysis, in a population of patients using an optimized dynamic contrast-enhanced imaging sequence and to estimate inter- and intra-patient variability. From these data to extract a representative AIF that may be used for realistic simulation studies.

Methods: Thirty-nine female patients were imaged on multiple visits before and during a course of neoadjuvant chemotherapy for breast cancer. A total of 97 T_1-weighted dynamic contrast-enhanced studies were analyzed including bookend estimates of T_1 and model-fitting to each individual AIF. Area under the curve and cardiac output were estimated from each first pass peak and these data were used to assess inter- and intra-patient variability of the AIF.

Results: Inter-patient variability exceeded intra-patient variability of the AIF. There was no change in cardiac output as a function of MR visit (mean value 5.6 ± 1.1 L/min) but baseline blood T_1 increased significantly following the start of chemotherapy (which was accompanied by a decrease in hematocrit).

Conclusion: The AIF in an individual patient can be measured reproducibly but the variability of AIFs between patients suggests that use of a population AIF will decrease the precision of tracer kinetic analysis performed in cross-patient comparison studies. A representative AIF is presented that is typical of the population but retains the characteristics of an individually measured AIF.

Key Words:

Introduction

Dynamic contrast-enhanced (DCE) MRI allows measurement of tissue hemodynamic characteristics by monitoring the delivery and distribution of an intravenously administered contrast agent, through its effect on the tissue's T_1 relaxation time. Techniques for analyzing DCE data are undergoing continuous adaptation and are becoming a valuable tool in oncology (e.g. for diagnosis and monitoring of cancer) and other conditions (e.g. in the brain and kidneys) [1-3]. In particular, the introduction of quantitative assessment triggered a cascade of applications and had a significant effect on the acquisition techniques used in DCE-MRI [4]. MR signal intensity changes, due to the distribution of the contrast agent in the tissue, form temporal features that depend on the tissue pathophysiology, the imaging sequence used and the administration protocol and properties of the contrast agent. Quantitative analysis with tracer kinetic modelling allows the characterization of tissue microvasculature (e.g. tissue blood flow, blood volume fraction) and provides information on the exchange of contrast agent between vascular and interstitial compartments.

In order to decouple the response of the tissue from the contrast agent administration protocol, tracer kinetic modelling requires the concentration of the contrast agent in the feeding arteries, also known as the arterial input function (AIF), to be determined. Ideally, the delivery of the contrast agent should be sampled from an artery that directly feeds the tissue of interest. Furthermore, the frequency with which the AIF is sampled has a significant impact on the accuracy and precision of the resulting parameter estimates and influences the choice of model [5,6]. The sampling rate is particularly important during the early phase following bolus administration, when the signal in blood exhibits large and rapid changes. These requirements impose certain spatio-temporal limitations on the acquisition protocol that are usually difficult to achieve. Furthermore, additional challenges such as partial volume, B_1 inhomogeneity, incomplete spoiling and inflow effects may reduce the quality of the AIF measurement further and propagate as errors in subsequent tracer kinetic parameter estimates [7,8].

It is common that the acquired data do not allow an AIF to be measured reliably. In these cases, an AIF is either assumed from the time course of the mean blood plasma concentration from a number of relevant studies (a population AIF) or extracted from a functional form of AIF [9-12]. One such approach, described by Parker et al. in 2006 [10], has proved to be very popular having been used numerous times for both simulation studies and data analysis. However, use of such approaches introduces limitations. The temporal details during the early bolus passes

may be distorted and individual variability (e.g. cardiac output, bolus injection duration and contrast agent dose) is lost [12]. Another proposed solution is the reference region approach [13,14], but this makes assumptions about the reference tissue; and the extracted AIF may feature different temporal characteristics than expected (i.e. lower and more dispersed first pass peak). Despite the alternative approaches, a reliably measured individual AIF is superior with respect to the accuracy of the parameter estimates [15-17].

It is essential to assess the repeatability of AIF measurement in order to understand the impact of using a population average AIF on subsequent tracer kinetic analysis. In this work we have used a high temporal resolution DCE-MRI acquisition protocol and measured AIFs from a population of thirty-nine patients with breast cancer undergoing neoadjuvant chemotherapy prior to surgical resection. The participants were scanned between 1 and 5 times before and during their therapy, resulting in a total of 97 datasets. Each individual AIF was fitted with a functional AIF form [12] and this was used to obtain a measurement of the area under the first pass peak from which we assessed intra- and inter-patient variability and hence examined the repeatability of AIF measurement in a population of patients. Finally, using the parameters estimated from the model, we present a representative AIF that retains the features of an individually measured AIF.

Methods

Patients

Thirty-nine female patients (median age = 44, range = 25 – 69 years) diagnosed with invasive breast cancer and due to undergo neoadjuvant chemotherapy prior to surgery were enrolled in this prospective study. The study was approved by a local research ethics committee and written informed consent was obtained from each patient. Blood samples, taken as part of normal standard of care, were used to measure the large vessel hematocrit (Hct) before each MRI scan. Patients with contraindications to MRI were excluded from the study.

MR imaging

All patients were scanned on a 1.5 T Aera MR scanner (Siemens, Erlangen, Germany), positioned head first prone, and data were acquired in the transverse plane using a bilateral breast coil. A flexible matrix coil was also positioned on the patients' backs to enhance the signal from the descending aorta. Before the dynamic acquisition, a 3D non-selective inversion recovery (IR) prepared spoiled gradient echo (FLASH) sequence (FOV: 340×340×180 mm,

matrix size: 128×128×36, IR-TR: 3000 ms, TR/TE: 2.8/0.93 ms, flip angle: 8°, GRAPPA parallel factor: 2, T_{acq}: 1 min 05 s per inversion time) was used at four inversion times (TI: 100, 600, 1200 and 2800 ms) for T_1 measurement. The accuracy of this approach was tested in a phantom study detailed in Supporting Information S1. The IR sequence was repeated immediately after the DCE-MRI experiment.

The dynamic series consisted of 93 high temporal resolution volumes interleaved with 8 high spatial resolution volumes (the latter were not used in our analysis but are part of the standard breast protocol used in our clinic), a variation of the acquisition scheme proposed by Georgiou et al. [18]. For the high temporal resolution dynamic data, a T_1-weighted 3D FLASH sequence (TR/TE: 2.37/0.73, FA: 25°, CAIPIRINHA parallel factor: 2×2, T_{acq}: 2 s) was employed with the same geometry used in the IR sequence. The volume selected encompassed both breasts, the heart, aortic arch and descending aorta (Figure 1).

Contrast agent

All patient studies followed the same contrast agent administration protocol. Gd-DOTA (Dotarem; Guerbet, Laboratories, Aulnays Sous Bois, France) was administered intravenously via the antecubital vein using an automated power injector (Spectris Solaris EP), at the beginning of the 11th dynamic volume (dose of 0.1 mmol/kg) followed by 20 ml of saline at a rate of 3 ml/s.

Postprocessing

Data were processed in PMI (Platform for Research in Medical Imaging, version 0.4 [19]) and Matlab (Mathworks, Nattick, MA, USA). For AIF extraction, regions of interest (ROIs) were drawn in the descending aorta and, for consistency across patients, were sampled in the same 10 slices (starting from inferior slices, ROIs were drawn in the 5th to 14th slices). Fig. 1 illustrates a representative example of the volume slab excited in our DCE-MRI experiment. The 3D ROIs were further trimmed to include only voxels that had a peak relative signal intensity change between the 50th and the 95th percentile of the signal change maxima [18]. These slices and percentiles were chosen empirically, to minimize inflow, section profile and partial volume artifacts. The median number of voxels included in the 3D ROIs for the AIF was 162 (range 87 – 358).

The ROIs extracted were used to sample the dynamic data to obtain the AIF time series and both sets of IR images to obtain a baseline and a post-contrast T_1 measurement, by fitting the

IR-FLASH signal equation [20,21] to the measured signal intensities at the four inversion times. Using the pair of T_1 estimates and the signal equation for a FLASH sequence [22], an iterative approach was followed to apply a bookend correction to the ΔR_1 (T_1 relaxation rate change) series, as described by Cron et al. [23]. To calculate the respective blood concentration time series for each patient a contrast agent relaxivity of 4.2 s^{-1} mM^{-1} was assumed [24]. As a last step, the extracted AIFs were time-shifted so that the contrast appeared at $t = 0$ and the data were truncated so that each AIF covered a period of approximately 4.5 minutes.

For subsequent analysis we used a functional form to fit to each AIF, to allow more accurate interpolation and integration of the first pass peak. Horsfield's model [12] was used since it provides a description of contrast agent recirculation, dispersion and redistribution that is based on physiological factors and because it can be fitted to individual AIF data sets, as opposed to an experimentally derived functional form that is fitted to averaged data from a population of subjects [10]. In our implementation of the Horsfield model, three exponential decay terms were used to characterize extravasation and excretion, combined with repeated gamma variate functions to account for recirculation. The equation for the period between the start of the nth recirculation and the $(n+1)^{th}$ recirculation, is given by:

$$C_p(t) = \left[\sum_{i=1}^{3} A_i e^{-m_i t}\right]\left[\sum_{j=0}^{n} \gamma\big((j+1)\alpha + j, \beta, t - j\tau\big)\right], \qquad n\tau < t < (n+1)\tau$$

$$\gamma(\alpha, \beta, t) = \frac{t^\alpha e^{-t/\beta}}{\beta^{(\alpha+1)}\Gamma(\alpha+1)}, \qquad\qquad t \geq 0 \qquad\qquad (1)$$

where A_i and m_i are the amplitudes and time constants of the exponential terms, the coefficients α and β reflect the number of "theoretical mixing chambers" and the ratio of the volume of the mixing chambers to the volume flow rate, and τ is the recirculation time. The gamma variate function takes the form given above for all $t \geq 0$ and is 0 for all $t < 0$.

Eqn. 1 was fitted to the individual AIFs using the Levenberg-Marquardt iterative least-squares optimization algorithm. Given the large number of fit parameters, we used multiple random initial estimates within a predefined range for each parameter. The first pass was isolated from Eqn. 1 and an analytical solution for the area under the first pass curve (AUC_{1st}) in terms of the fitting parameters was derived (Eqn. 2)

$$AUC_{1st} = \sum_{i=1}^{3} \frac{A_i}{\beta^{\alpha+1}}\left(m_i + \frac{1}{\beta}\right)^{-(\alpha+1)} \qquad\qquad (2)$$

Furthermore, using indicator dilution principles [25] we generated an estimate of the patient's cardiac output (CO) from each AIF

$$CO = {}^{D}\!/_{AUC_{1st}} \tag{3}$$

where D is the dose of injected contrast agent, estimated by multiplying the concentration of Gd-DOTA used (0.5 mmol/ml) by the volume of contrast agent administered.

Repeatability Assessment

To assess the repeatability of AIF measurement in the patient cohort, we examined the variability in pre-contrast T_1, AUC_{1st} and CO estimates. In addition, we assessed variability of Hct. These were first assessed for normality using the Shapiro-Wilk test and a Q—Q (quantile-quantile) plot. One-way analysis of variance (ANOVA) for repeated measurements was used to test for any significant changes across MRI visits and to estimate inter- and intra-patient coefficients of variability (CV). To select a representative AIF we first fitted the population average AIF using Equation 1, and then identified the individual AIF whose first pass profile was closest to that of the population average AIF, using the least square differences of the two time series. The respective parameter estimates from the individual patient were used to generate a representative AIF.

Results

In this study we analyzed 97 datasets from thirty-nine patients who underwent a total of 146 MR examinations. Datasets were excluded due to: missing back coil, motion-corrupted AIF, deviation from the standard injection protocol (e.g. manual injection or slower injection) or missing IR data. Figure 2a shows the population-averaged AIF from all available datasets. The discontinuities in this plot are due to the interleaved acquisition scheme used [18]. Furthermore, although the number of DCE volumes was fixed for all scans, some data appear in the gaps because of the effect of variable time shifts.

Figure 2b demonstrates how Horsfield's model is implemented, with each recirculation (illustrated with a different color) progressing with the amount of contrast agent remaining from the previous pass plus that which is recirculated. An example of the individual AIFs and associated fits are also shown in Figure 3 for a patient who underwent four MR examinations.

The resulting model parameters were used in Eqn. 2 to estimate AUC_{1st}. Table 1 shows the estimates obtained for pre-contrast blood T_1, Hct, AUC_{1st}, and CO. Figure 4 demonstrates the variability of these estimates within and between visits. All data followed a normal distribution ($p > 0.05$, Shapiro-Wilk test) and the results of the ANOVA test (Table 2) suggest that there were no significant differences between visits for both AUC_{1st} ($p = 0.77$) and CO ($p = 0.70$). There was a significant difference in the blood T_1 estimates ($p < 0.001$) with a step increase between visit 1 (pre-chemotherapy) and visits 2, 3 and 4 (all during chemotherapy). Similarly, Hct showed a significant change across visits ($p < 0.001$), with a decrease seen at visits 3, 4 and 5 compared to baseline.

For both AUC_{1st} and CO variability within patients (total mean squares, MS = 0.01 mM·min and 0.29 L/min, respectively) was lower than variability between patients (MS = 0.16 mM·min and 2.45 L/min, respectively). Similarly, the inter- and intra-patient CV were estimated to be 21% and 11% for AUC_{1st}, 17% and 11% for CO, 7.7% and 7.1% for Hct and 4.6% and 4.2% for T_1.

Figure 5 illustrates the representative AIF from this patient cohort plotted alongside the population AIF from [10]. The fitted parameters are shown in Table 3 and an Excel file of the respective time series, at a high temporal resolution (0.1 s), is provided as Supporting Information S2. The AIF was measured following a bolus administration of 14.4 ml of Gd-DOTA at 3 ml/s followed by 20 ml of saline, from a female patient, aged 59 years with an Hct of 0.35 and a mass of 72 kg.

Discussion

In 2006 Parker et al. published a population-averaged AIF [10] that has subsequently been used by numerous investigators for both simulations and data analysis. Since then, DCE-MRI acquisition has improved allowing many of the limitations of that study to be addressed. We measured an AIF in 97 separate MRI studies obtained from a population of 39 patients. Our AIF measurements were performed at a high sampling rate (2 s per acquisition compared with 5 s previously [10]) using a flexible coil to enhance the signal from the descending aorta and to allow for a detailed characterization of the first pass and subsequent recirculations of the contrast agent bolus in the blood. Another strength of this protocol was the use of bookend IR T_1 measurements, which have been shown to improve the accuracy with which contrast agent concentration is estimated [26].

In Figure 2 we show a plot of the population-average AIF from all studies alongside an example AIF from an individual study. It is clear that the detailed temporal characteristics of the second pass seen in the individual AIF are lost in the population average AIF. Moreover, the majority of the individual AIFs examined in this study were characterized by a third pass peak, which is smoothed over in the population-average AIF. Incomplete sampling of the early bolus passes has been shown to introduce significant errors and fit failures in quantitative tracer kinetic analysis of tissue curves [18]. The different characteristics of the individual and population-average AIFs are likely the reason why Parker's population-average functional form failed to converge to satisfactory fits on individual AIFs [12]. Parker's model uses two Gaussians to account for the first pass and the second recirculation peak. Horsfield's recirculation model is able to capture multiple passes despite having fewer fit parameters (9 versus 10 parameters).

Using Eqn.3 we estimated AUC_{1st} in order to examine the variability of the AIFs for this patient cohort. Within patients there were no significant differences in AUC_{1st} between MRI visits. Furthermore, both MS and CV estimates for inter-patient variability were higher than for intra-patient variability. The 21% inter-patient CV suggests that use of a population average AIF will introduce additional variability and thus potentially limit the sensitivity of quantitative analysis across patients. Using AUC_{1st} we estimated CO, as described by Yang et al. [14]. The mean CO estimate was in good agreement with that measured in patients at rest and lying prone [27], providing indirect support for the accuracy of our measured AIFs. As noted by Yang, if the population-averaged AIF described by Parker is used to estimate CO, it results in an unrealistically high value (10.5 L/min) [14]. This may be due principally to under-sampling of the first pass leading to underestimation of AUC_{1st} [14] but will also have been affected by B_1 and inflow artifacts. This suggests that use of Parker's population AIF in quantitative analysis may introduce systematic overestimation of tracer kinetic model parameters.

Our baseline blood T_1 estimates match very well those recently reported in the literature at 1.5 T. For example, Dabir et al. provided estimates of 1551 ± 115 ms and 1572 ± 111 ms for blood T_1 from 102 healthy volunteers and 113 low-risk patients, respectively, of whom 51% were males [28]. Further studies in female subjects report blood T_1 values of 1667 ± 77 ms (n = 20 healthy females, [29]), 1664 ± 62 ms (n = 38 healthy females, [30]) and 1666 ± 77 ms (n = 65 females with at least one risk factor for heart failure, [30]). A factor that affects blood T_1 is Hct, which has been shown to account for the differences seen between female and male subjects; our patient cohort included female patients only and we saw a weak negative correlation between Hct and T_1 (r = -0.27, p = 0.006). Chemotherapy can have an impact on Hct; there was

a significant decrease in Hct for visits 3, 4 and 5 and an increase in T_1 for visits 2, 3 and 4 in comparison with visit 1 ($p < 0.005$).

In this study we used an optimized acquisition protocol to measure the AIF in a group of patients with breast cancer undergoing neoadjuvant chemotherapy. Our aim was to reduce variations caused by experimental measurement errors to examine variations that are inherent to individual patients. To achieve this, we used the same dose of contrast agent for all patients and the administration protocol was fixed. Data were acquired at a temporal resolution that was appropriate to sample the early bolus passes of the AIF and the use of a flexible coil on the patient's back enhanced the SNR from the aorta. Measurement errors related to inflow effects [7] were addressed by careful placement of the imaging volume to encompass heart, aortic arch, a significant region of lung tissue as well as descending aorta which also helped to reduce partial volume artifacts - Parker et al. used only a single slice and included data from the iliac arteries [10]. We have used a T_1 measurement technique based on a non-selective inversion recovery sequence, which is less prone to errors than a variable flip angle acquisition, and a bookend T_1 method to improve the accuracy of estimates of contrast agent concentration [23,26]. The result is a series of AIFs with excellent intra-patient repeatability but that highlight larger inter-patient variability. We provide the parameters of a functional form of a representative AIF from the patient cohort that would be ideal for simulation studies or intra-patient comparisons. For inter-patient comparisons reliable individual AIFs should be measured, where possible. If not, the use of a representative AIF may be necessary but is likely to decrease the precision of tracer kinetic analysis.

References

1. Padhani AR. Dynamic contrast-enhanced MRI in clinical oncology: current status and future directions. J Magn Reson Imaging 2002;16(4):407-422.
2. Gribbestad IS, Gjesdal KI, Nilsen G, Lundgren S, Hjelstuen MHB, Jackson A. An Introduction to Dynamic Contrast-Enhanced MRI in Oncology. In: Jackson A, Buckley DL, Parker GJM, editors. Dynamic Contrast-Enhanced Magnetic Resonance Imaging in Oncology. Berlin, Heidelberg: Springer Berlin Heidelberg; 2005. p 1-22.
3. Georgiou L, Buckley DL. T1-weighted DCE MRI. In: Cercignani M, Dowell N, Tofts PS, editors. Quantitative MRI of the Brain. 2 ed. Baco Raton: CRC Press; 2018. p 251-268.
4. Sourbron SP, Buckley DL. Tracer kinetic modelling in MRI: estimating perfusion and capillary permeability. Phys Med Biol 2012;57(2):R1-R33.
5. Henderson E, Rutt BK, Lee TY. Temporal sampling requirements for the tracer kinetics modeling of breast disease. Magn Reson Imaging 1998;16(9):1057-1073.
6. Cramer SP, Larsson HB. Accurate determination of blood-brain barrier permeability using dynamic contrast-enhanced T1-weighted MRI: a simulation and in vivo study on healthy subjects and multiple sclerosis patients. J Cereb Blood Flow Metab 2014;34(10):1655-1665.
7. Roberts C, Little R, Watson Y, Zhao S, Buckley DL, Parker GJ. The effect of blood inflow and B(1)-field inhomogeneity on measurement of the arterial input function in axial 3D spoiled gradient echo dynamic contrast-enhanced MRI. Magn Reson Med 2011;65(1):108-119.
8. Garpebring A, Wirestam R, Ostlund N, Karlsson M. Effects of inflow and radiofrequency spoiling on the arterial input function in dynamic contrast-enhanced MRI: A combined phantom and simulation study. Magn Reson Med 2011;65(6):1670-1679.
9. Tofts PS, Kermode AG. Measurement of the blood-brain barrier permeability and leakage space using dynamic MR imaging. 1. Fundamental concepts. Magn Reson Med 1991;17:357-367.
10. Parker GJ, Roberts C, Macdonald A, Buonaccorsi GA, Cheung S, Buckley DL, Jackson A, Watson Y, Davies K, Jayson GC. Experimentally-derived functional form for a population-averaged high-temporal-resolution arterial input function for dynamic contrast-enhanced MRI. Magn Reson Med 2006;56(5):993-1000.
11. Orton MR, Miyazaki K, Koh DM, Collins DJ, Hawkes DJ, Atkinson D, Leach MO. Optimizing functional parameter accuracy for breath-hold DCE-MRI of liver tumours. Phys Med Biol 2009;54(7):2197-2215.
12. Horsfield MA, Thornton JS, Gill A, Jager HR, Priest AN, Morgan B. A functional form for injected MRI Gd-chelate contrast agent concentration incorporating recirculation, extravasation and excretion. Phys Med Biol 2009;54(9):2933-2949.
13. Yankeelov TE, Luci JJ, Lepage M, Li R, Debusk L, Lin PC, Price RR, Gore JC. Quantitative pharmacokinetic analysis of DCE-MRI data without an arterial input function: a reference region model. Magn Reson Imaging 2005;23(4):519-529.
14. Yang C, Karczmar GS, Medved M, Oto A, Zamora M, Stadler WM. Reproducibility assessment of a multiple reference tissue method for quantitative dynamic contrast enhanced-MRI analysis. Magn Reson Med 2009;61(4):851-859.
15. McGrath DM, Bradley DP, Tessier JL, Lacey T, Taylor CJ, Parker GJ. Comparison of model-based arterial input functions for dynamic contrast-enhanced MRI in tumor bearing rats. Magn Reson Med 2009;61(5):1173-1184.

16. Port RE, Knopp MV, Brix G. Dynamic contrast-enhanced MRI using Gd-DTPA: Interindividual variability of the arterial input function and consequences for the assessment of kinetics in tumors. Magn Reson Med 2001;45(6):1030-1038.

17. Yankeelov TE, Cron GO, Addison CL, Wallace JC, Wilkins RC, Pappas BA, Santyr GE, Gore JC. Comparison of a reference region model with direct measurement of an AIF in the analysis of DCE-MRI data. Magn Reson Med 2007;57(2):353-361.

18. Georgiou L, Sharma N, Broadbent DA, Wilson DJ, Dall BJ, Gangi A, Buckley DL. Estimating breast tumor blood flow during neoadjuvant chemotherapy using interleaved high temporal and high spatial resolution MRI. Magn Reson Med 2018;79(1):317-326.

19. Sourbron S, Biffar A, Ingrisch M, Fierens Y, Luypaert R. PMI: platform for research in medical imaging. Magn Reson Mater Phy 2009;22(1):539.

20. Brix G, Schad LR, Deimling M, Lorenz WJ. Fast and Precise T1 Imaging Using a Tomrop Sequence. Magn Reson Imaging 1990;8(4):351-356.

21. Kershaw LE, Hutchinson CE, Buckley DL. Benign prostatic hyperplasia: evaluation of T1, T2, and microvascular characteristics with T1-weighted dynamic contrast-enhanced MRI. J Magn Reson Imaging 2009;29(3):641-648.

22. Haase A. Snapshot FLASH MRI - applications to T1, T2, and chemical-shift imaging. Magn Reson Med 1990;13:77-89.

23. Cron GO, Santyr G, Kelcz F. Accurate and rapid quantitative dynamic contrast-enhanced breast MR imaging using spoiled gradient-recalled echoes and bookend T-1 measurements. Magn Reson Med 1999;42(4):746-753.

24. Rohrer M, Bauer H, Mintorovitch J, Requardt M, Weinmann HJ. Comparison of magnetic properties of MRI contrast media solutions at different magnetic field strengths. Invest Radiol 2005;40(11):715-724.

25. Stewart GN. Researches on the Circulation Time and on the Influences which affect it. J Physiol 1897;22(3):159-183.

26. Cron GO, Kelcz F, Santyr GE. Improvement in breast lesion characterization with dynamic contrast-enhanced MRI using pharmacokinetic modeling and bookend T(1) measurements. Magn Reson Med 2004;51(5):1066-1070.

27. Dharmavaram S, Jellish WS, Nockels RP, Shea J, Mehmood R, Ghanayem A, Kleinman B, Jacobs W. Effect of prone positioning systems on hemodynamic and cardiac function during lumbar spine surgery: an echocardiographic study. Spine (Phila Pa 1976) 2006;31(12):1388-1393.

28. Dabir D, Child N, Kalra A, Rogers T, Gebker R, Jabbour A, Plein S, Yu CY, Otton J, Kidambi A, McDiarmid A, Broadbent D, Higgins DM, Schnackenburg B, Foote L, Cummins C, Nagel E, Puntmann VO. Reference values for healthy human myocardium using a T1 mapping methodology: results from the International T1 Multicenter cardiovascular magnetic resonance study. J Cardiovasc Magn Reson 2014;16:69.

29. Reiter U, Reiter G, Dorr K, Greiser A, Maderthaner R, Fuchsjager M. Normal diastolic and systolic myocardial T1 values at 1.5-T MR imaging: correlations and blood normalization. Radiology 2014;271(2):365-372.

30. Pagano JJ, Chow K, Paterson DI, Mikami Y, Schmidt A, Howarth A, White J, Friedrich MG, Oudit GY, Ezekowitz J, Dyck J, Thompson RB. Effects of age, gender, and risk-factors for heart failure on native myocardial T1 and extracellular volume fraction using the SASHA sequence at 1.5T. J Magn Reson Imaging 2018; DOI:10.1002/jmri.26160.

31. Weinmann HJ, Laniado M, Mutzel W. Pharmacokinetics of Gd-DTPA/dimeglumine after intravenous injection into healthy volunteers. Physiol Chem Phys Med NMR 1984;16:167-172.
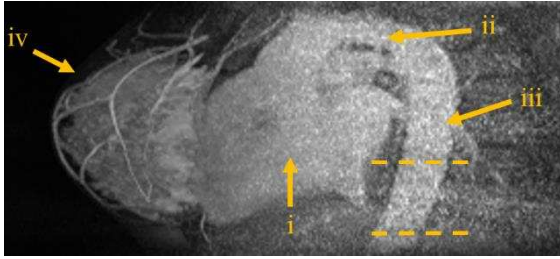
Figures

Figure 1. Example of the MRI volume slab acquired for the DCE data, which included the (i) heart, (ii) aortic arch, (iii) descending aorta and (iv) breasts. The image represents a maximum intensity projection in the sagittal plane. This was generated after subtracting the pre-contrast high spatial resolution volume from the first post-contrast high spatial resolution volume, and reconstructing the images in the sagittal plane. The dashed lines demonstrate the region where the AIF was sampled.
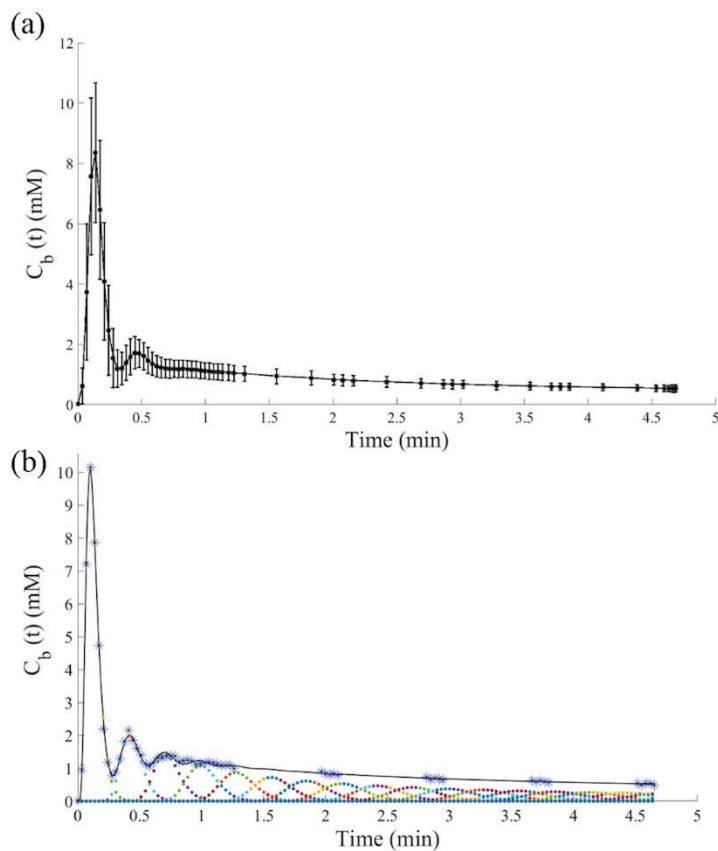

Figure 2. (a) Average AIF with error bars (± one standard deviation) across 97 individual AIFs. Note that the gaps in the time series are due to the interleaved acquisition scheme and averaging

data points on each side of successive acquisition bursts. (b) Example of Horsfield's functional form fitted to an individual AIF. The black solid line indicates the fitted line through the data (asterisks). The colored data points indicate the recirculation phases of the contrast agent.
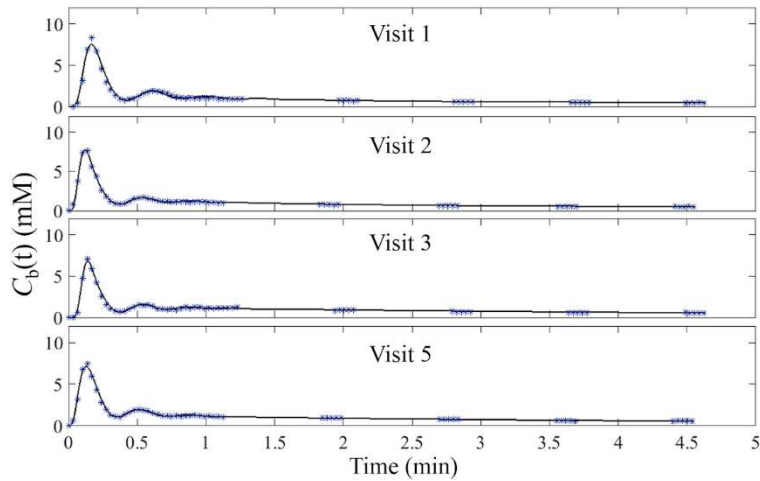

Figure 3. Measured AIFs (asterisks) and individual fits (solid lines) from one patient over four MRI visits. The estimated CO was 4.56, 5.05, 6.02 and 4.98 L/min at visits 1 to 4 (patient age: 39 years, weight: 63.5 kg at each visit, volume of Gd-DOTA administered: 12.7 ml at each visit).
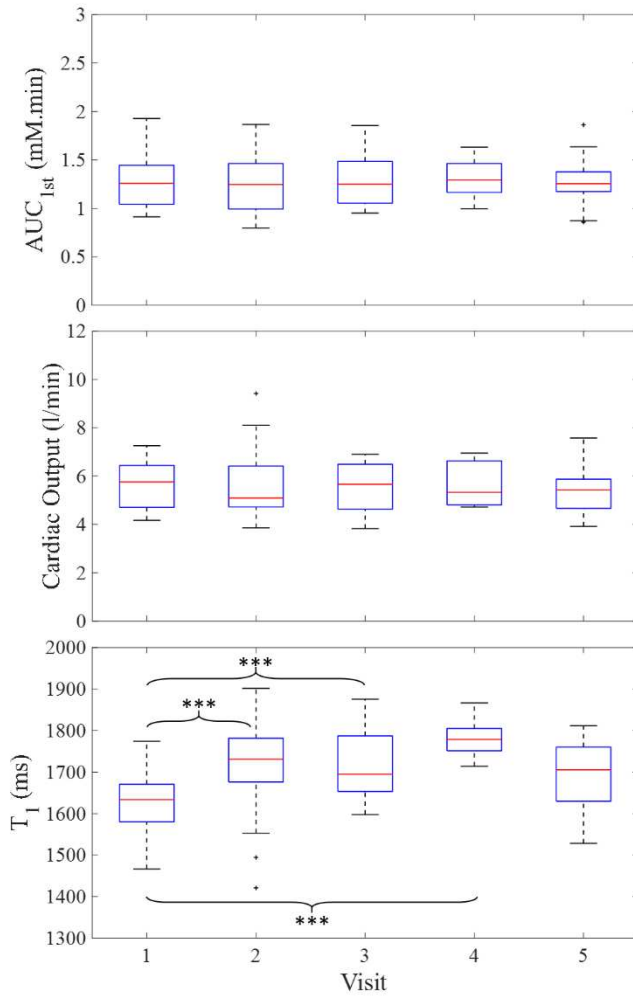
Figure 4. Boxplots of AUC$_{1st}$, CO and pre-contrast blood T$_1$ as a function of MRI visit. The box represents the middle 50% of values for the visit, and the upper and lower whiskers the complete range. *** denotes a significant difference at the 95% significance level.
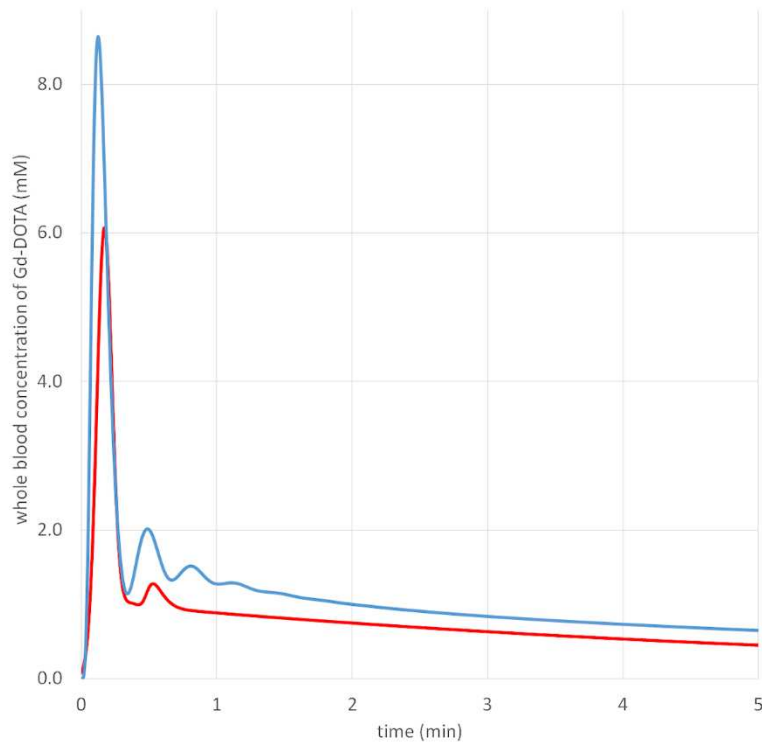
Figure 5. A representative AIF from this patient cohort (blue line) that was obtained from a 59 year old female with a body weight of 72 kg, receiving a bolus of 14.4 ml of Gd-DOTA (dose of 0.1 mmol/kg) administered at a rate of 3 ml/s and followed by 20 ml of saline. The patient's Hct at the time of the scan was 0.35 and estimated CO from this AIF was 5.2 L/min. The population AIF of Parker et al. [10] is shown alongside for comparison (red line), and when converted to plasma concentration the representative AIF converges with the data presented by Weinmann et al [31] by ~10 mins post-injection.

Table 1. Blood T_1, AUC_{1st} and CO estimates for each MR visit.

Parameters	Visit 1 baseline (n=29) Mean ± σ	Visit 2 post-cycle 1 (n=25) Mean ± σ	Visit 3 post-cycle 3 (n=20) Mean ± σ	Visit 4 post-cycle 5 (n=5) Mean ± σ	Visit 5 after chemotherapy (n=18) Mean ± σ	Overall (n=97) Mean ± σ
Blood T_1 (ms)	1626 ± 72	1718 ± 107	1716 ± 80	1782 ± 55	1696 ± 82	1689 ± 95
Hematocrit	0.41 ± 0.02	0.39 ± 0.03	0.37 ± 0.03	0.35 ± 0.04	0.36 ± 0.02	0.38 ± 0.03
AUC_{1st} (mM.min)	1.28 ± 0.28	1.26 ± 0.32	1.28 ± 0.25	1.31 ± 0.23	1.29 ± 0.25	1.28 ± 0.27
CO (L/min)	5.66 ± 0.93	5.68 ± 1.38	5.49 ± 1.01	5.67 ± 1.01	5.53 ± 1.13	5.61 ± 1.10

Table 2. Results of the one-way ANOVA for repeated measures.

Source	df	AUC$_{1st}$ (mM.min) Partial SS	MS	F	p	CO (L/min) Partial SS	MS	F	p	T_1 (ms) Partial SS	MS	F	p	Hct Partial SS	MS	F	p
Patient ID	30	5.55	0.19			82.63	2.75			329466	10982			0.035	0.001		
MRI visit	4	0.05	0.01	0.46	0.77	1.17	0.29	0.55	0.7	126741	31685	5.86	0.001*	0.033	0.008	19.69	<0.001*
Residual	62	1.58	0.03			32.79	0.53			335108	5405			0.026	0.000		
Total	96	7.15	0.07			116.08	1.21			859547	8954			0.100	0.001		

df – degrees of freedom, MS – Mean Squares, SS – sum of squares, * denotes significance at 95% level

Table 3. Parameter estimates for the functional form of the representative AIF.

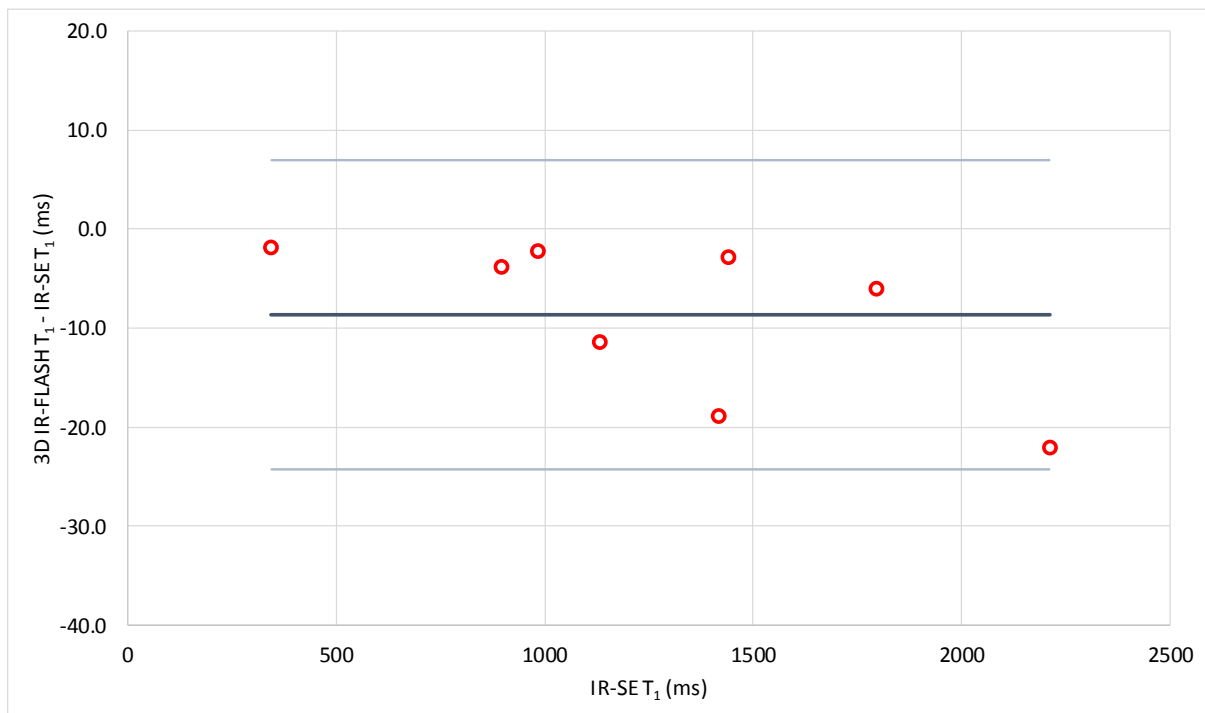| Parameter	A_1	m_1	A_2	m_2	A_3	m_3	α	β	τ
Value	0.37	0.11	0.33	1.17	10.06	16.02	5.26	0.032	0.129
Unit	mM	min^{-1}	mM	min^{-1}	mM	min^{-1}	-	min	min

Supporting Information S1. Details of a phantom experiment performed to test the accuracy of the 3D IR-FLASH sequence for blood T_1 measurement.

Supporting Information Figure S1. Bland-Altman plot of the difference between 3D IR-FLASH estimates of T_1 and IR-SE estimates of T_1 against IR-SE T_1 in the HCMR phantom. Horizontal lines representing mean bias (bold) and ±95% confidence intervals (faint lines) are shown.

Supporting Information S2. A spreadsheet containing data describing the representative AIF derived from this patient cohort. It was calculated using Eqn. 1 and the parameters listed in Table 3 which were estimated from a best-fit to data obtained from a 59 year old female with a body weight of 72 kg, receiving a bolus of 14.4 ml of Gd-DOTA (dose of 0.1 mmol/kg) administered at a rate of 3 ml/s and followed by 20 ml of saline. The patient's Hct at the time of the scan was 0.35 and estimated CO from this AIF was 5.2 L/min.

Supporting Information S1 – Details of a phantom experiment performed to test the accuracy of the 3D IR-FLASH sequence for blood T_1 measurement.

We imaged the Hypertrophic Cardiomyopathy Registry (HCMR) phantom and assessed gels with T_1 values in the range 344 to 2211 ms (measured in the same session using a single slice IR-spin echo (SE) sequence with a TR of 10 s and 8 TI times: 100, 200, 400, 800, 1600, 3200, 6400 & 9000 ms). Results using the 3D IR-FLASH sequence with the acquisition parameters detailed in the main manuscript (IR-TR: 3000 ms, TR/TE: 2.8/0.93 ms, flip angle: 8°, GRAPPA parallel factor: 2, four inversion times: 100, 600, 1200 and 2800 ms) were excellent. The 3D IR-FLASH sequence produced results with a mean bias of -9 ms and 95% confidence intervals of -24 to +7 ms.

Supporting Information Figure S1. Bland-Altman plot of the difference between 3D IR-FLASH estimates of T_1 and IR-SE estimates of T_1 against IR-SE T_1 in the HCMR phantom. Horizontal lines representing mean bias (bold) and ±95% confidence intervals (faint lines) are shown.